Electronic Supplementary Material (ESI) for Journal of Materials Chemistry A.

Electronic Supporting Information

Multistage Coupling of Interface and Core-shell Engineering of Cobalt-Based Heterostructure for Integration of Multiple Electromagnetic Absorption

*Jun Zhou, Hu Guo, Jun Di, Guigao Liu and Wei Jiang**

National Special Superfine Powder Engineering Technology Research Center,

Nanjing University of Science and Technology, Nanjing 210094, Jiangsu, China

**Corresponding author: superfine_jw@126.com (Wei Jiang)*

Experimental

Synthesis of ZIF-67 nanocube

First, 5mg cetyltrimethylammonium bromide (CTAB) was dissolved in 10 mL deionized water (DIW). Second, 292 mg of cobalt nitrate hexahydrate was added to form solution A. Third, 4.52 g of dimethylimidazole was dissolved in 70 mL of DIW to form solution B. Fourth, the B solution was quickly poured into the A solution and stirred for 40 min at room temperature. The product was obtained by centrifugation, washed three times with methanol and DIW alternately, and finally dried at 60 °C overnight.

Synthesis of GO/ZIF-67

The GO/ZIF-67 were fabricated by the same procedure of ZIF-67, except that the first step. Specifically, 30 mg GO was added to 30 mL DIW and ultrasonically dispersed to form solution A. Second, 5 mg CTAB was dissolved in 10 mL DIW, and 292 mg cobalt nitrate hexahydrate was added to form solution B. Thirdly, solution B was added to solution A and stirred for 30 min. The subsequent procedure is the same as the above procedure.

Synthesis of PDA/GO/ZIF-67

Typically, 0.1 g of Pluronic F-127 and 100 mg of dopamine hydrochloride were dissolved in a mixed solvent (20 mL DIW and 20 mL ethanol solution) and stirred for 10 min. Second, 100 mg GO/ZIF-67 was added to the above solution and stirred for 30 min. Thirdly, Tris (2 mL, 0.1323 g) solution was added dropwise to the mixture to promote polymerization. Fourth, continue to stir the mixture at room temperature for

5h. The products were collected by centrifugation, washed with DIW, and finally dried in vacuum at 60 °C overnight.

PDA/ZIF-67 were prepared by the same procedures except replacing GO/ZIF-67 with ZIF-67.

PDA/GO were prepared by the same procedures except replacing GO/ZIF-67 with GO.

Synthesis of N-PC@IC/Co/rGO

The N-PC@IC/Co-rGO was obtained by pyrolysis procedure. Representatively, 200 mg of PDA/GO/ZIF-67 were placed into a tube furnace and then annealed at 700 °C for 2h with a heating rate of 3 °C/min under N_2 atmosphere.

The other products were fabricated by the same procedure except replacing the precursor.

Characterization

The morphology of the samples is measured by Field-emission scanning electron microscope (FESEM; Hitachi Regulus 8100) and transmission electron microscopy (TEM; FEI Tecnai F20). HAADF-STEM images were captured with equipped with a cold field-emission gun. The STEM energy-dispersive X-ray (EDX) spectroscope was collected and processed in an Oxford Aztec EDS system. X-ray diffraction (XRD; Rigaku D/max-2200PC) with Cu Kα radiation is employed to record the crystal structure of the samples. Fourier transform infrared spectroscopy (FTIR; Thermo Scientific Nicolet iS20) is employed to study the surface functional groups of the samples. Raman spectra were obtained using a Raman spectrometer (Horiba LabRAM

HR Evolution) at room temperature using the 532 nm line as the excitation source. The detailed electronic structure of the samples is measured by X-ray photoelectron spectroscopy (XPS; ESCALAB 250Xi, Thermo Scientific K-Alpha), where the binding energy of 284.6 eV for the adventitious carbon (C 1s) is used as the reference. Magnetization was measured by using a vibrating sample magnetometer (VSM; Lakeshore7404) at room temperature. The conductivity were measured on the resistance meter by the four-segment method (Jingge-ST2643). The adsorption-desorption isotherm is obtained by the specific surface area analyzer (Micromeritics ASAP 2460).

Electromagnetic parameters

The electromagnetic parameters (real and imaginary parts of permittivity and permeability) of the sample were obtained by the network analyzer (AV3672B-S) at the 2-18 GHz. The sample preparation were divided into three steps. First, evenly mix the sample with molten paraffin. To obtain the electromagnetic properties of the samples, the powders were uniformly mixed with molten paraffin in proportions. Then, natural curing. Finally, the mixtures were pressed into a cylindrical shape with a mold, with an inner diameter of 3.04 mm, an outer diameter of 7 mm and thicknesses of 2-3 mm.

Based on the transmission line theory, the reflection loss (RL) can be calculated by the following equations:[1,2]

$$RL\ (dB)\ = 20\lg\left|\frac{Z_{in} - Z_0}{Z_{in} + Z_0}\right| \quad (1)$$

$$Z_{in} = Z_0\left(\mu_r/\varepsilon_r\right)^{1/2}\tanh\left[j(2\pi f d/c)\left(\mu_r\varepsilon_r\right)^{1/2}\right] \quad (2)$$

where Z_{in} is the input impedance of a single layer of absorbing material, Z_0 is the free space impedance, ε_r is the complex permittivity, μ_r is the complex permeability, f is the test frequency and d is the thickness of the absorbing material.

The imaginary part of permittivity can be analyzed via the free electron theory, which is described by the following equation:

$$\varepsilon'' \approx 1/2\pi\varepsilon_0\rho f \quad (3)$$

According to the Debye theory, the dielectric loss can be depicted by the following equations:[3,4]

$$\varepsilon' = \varepsilon_\infty + \frac{\varepsilon_s - \varepsilon_\infty}{1+\omega^2\tau^2} \quad (4)$$

$$\varepsilon'' = \frac{\varepsilon_s - \varepsilon_\infty}{1+\omega^2\tau^2}\omega\tau + \frac{\sigma}{\omega\varepsilon_0} \quad (5)$$

$$\left(\varepsilon' - \frac{\varepsilon_s + \varepsilon_\infty}{2}\right)^2 + (\varepsilon'')^2 = \left(\frac{\varepsilon_s + \varepsilon_\infty}{2}\right)^2 \quad (6)$$

where ε_s is the stationary dielectric constant, ε_∞ represents the optical dielectric constant, ω is the angular frequency, τ is the relaxation time and σ is the electrical conductivity.

The attenuation constant (α) can be described as:[5,6]

$$\alpha = \frac{\sqrt{2}\pi f}{c} \times \sqrt{(\mu''\varepsilon'' - \mu'\varepsilon') + \sqrt{(\mu''\varepsilon'' - \mu'\varepsilon')^2 + (\mu'\varepsilon'' + \mu''\varepsilon')^2}} \quad (7)$$

where c is the velocity of light in free space.

According to Maxwell-Garnett theory:[7,8]

$$\varepsilon_{eff}^{MG} = \varepsilon_1\frac{(\varepsilon_2 + 2\varepsilon_1) + 2f_v(\varepsilon_2 - \varepsilon_1)}{(\varepsilon_2 + 2\varepsilon_1) - f_v(\varepsilon_2 - \varepsilon_1)} \quad (8)$$

where (ε_{eff}^{MG}) is the effective permittivity of material, (ε_1) is the solid permittivity and (ε_2) is void permittivity.

The experimental absorption thickness (t_m) and corresponding absorption frequency (f_m), which can be satisfied through the following conditions:[9,10]

$$t_m = \frac{n\lambda}{4} = \frac{nc}{4f_m\sqrt{|\mu_r\varepsilon_r|}} (n = 1,3,5\ldots) \quad (9)$$

The impedance matching can be expressed as follows:[11,12]

$$Z = \left|Z_{in}/Z_0\right| = \left(\mu_r/\varepsilon_r\right)^{1/2}\tanh\left[j(2\pi fd/c)\left(\mu_r\varepsilon_r\right)^{1/2}\right] \quad (10)$$

Density functional theory calculation method

All density functional theory (DFT) calculations were performed by the first-principles within the generalized gradient approximation (GGA) using the Perdew-Burke-Ernzerhof (PBE) formulation.[13,14] The ionic cores were described by the projected augmented wave (PAW) potentials, and the valence electrons are considered to use a plane wave basis set with a kinetic energy cutoff of 450 eV.[15] Partial occupancies of the Kohn−Sham orbitals were allowed using the Gaussian smearing method and a width of 0.05 eV.[16] Electron energy self-consistency is considered when the energy change is less than 10^{-5} eV. A geometry optimization was considered convergent when the energy change was smaller than 0.02 eV/Å. The 18 Å vacuum layer was normally added to the surface to eliminate the artificial interactions between periodic images. The Brillouin zone was integrated with a Monkhorst-Pack 5×3×1 k-point grid for (density of states calculation. The Dipole correction taken into account for this calculation.

Radar cross section simulation

High Frequency Structure Simulator (HFSS 15.0) was used to simulate the radar cross section of the as-prepared absorbers. The metal substrate is defined as a perfect conductor (because of the wavelength corresponding to the simulation frequency is much smaller than the size of the metal substrate) with a size of 180*180*5 mm based on the widely accepted metal substrate model. Specifically, the thickness of the absorber above the metal substrate was set to an optimum thickness (N-IC/Co: 5.0 mm; N-PC@IC/Co: 2.0 mm; N-IC/Co/rGO: 5.0 mm; N-PC@IC/Co/rGO: 2.52 mm), and length for each side are set as 180 mm. Model-Driven solution was determined as the simulation solution for this work. The model was placed on the X-Y-Z plane, defining the excitation mode of the plane wave, with normal incidence from the Z axis. The plane wave incidence direction is determined by theta and phi in spherical coordinates. Herein, the incident directions of the plain wave was described as theta=0° and phi=0°. Besides, the operating frequency was determined as 9 GHz corresponding to the optimal absorption properties. Radiation Boundary is set as the boundary condition of this work, where the boundary size is defined as 200 * 200 mm (the boundary size should be greater than a quarter of the operating frequency wavelength, set to 20 mm).

Typically, the metal substrate RCS calculation equation can be expressed as:[17,18]

$$\sigma(dBm^2) = \lim_{R\to\infty} 4\pi R^2 \frac{|E_s|^2}{|E_i|^2} = \lim_{R\to\infty} 4\pi R^2 \frac{|H_s|^2}{|H_i|^2} \quad (11)$$

where R is the distance between the target and the incident source, E_s and H_s are the scattering electric field and the scattering magnetic field intensity respectively, E_i and

H_i are the incident electric field intensity and the incident magnetic field intensity, respectively.

Results and discussion

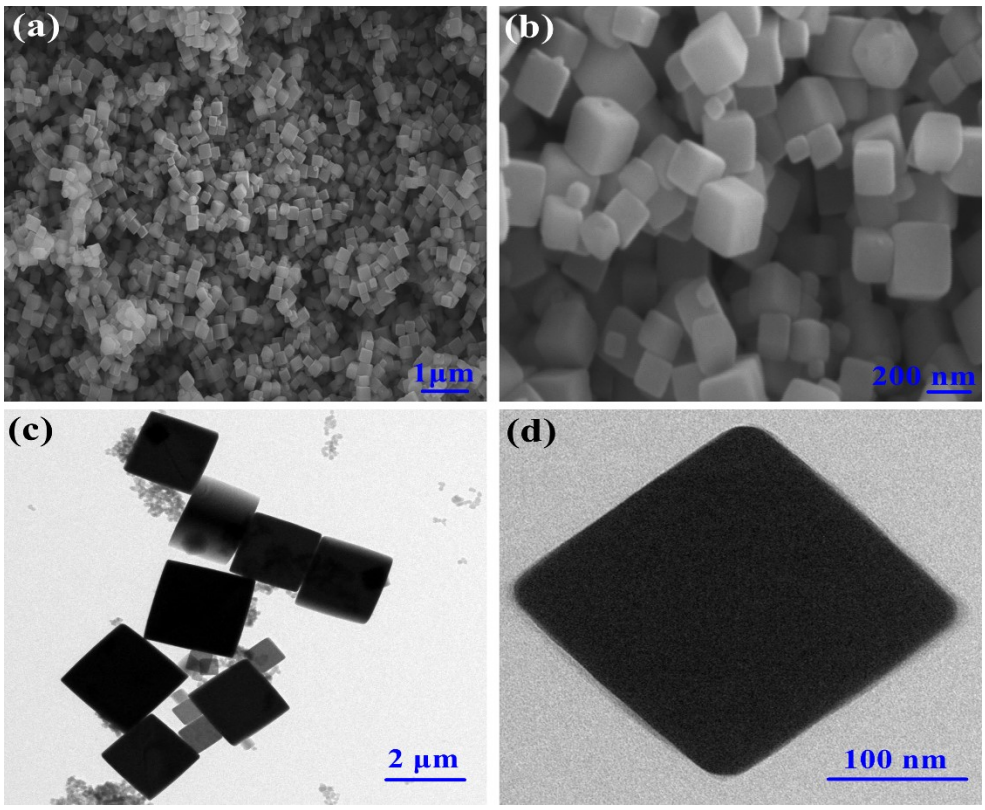

Fig. S1. (a,b) SEM and (c,d) TEM images of the ZIF-67

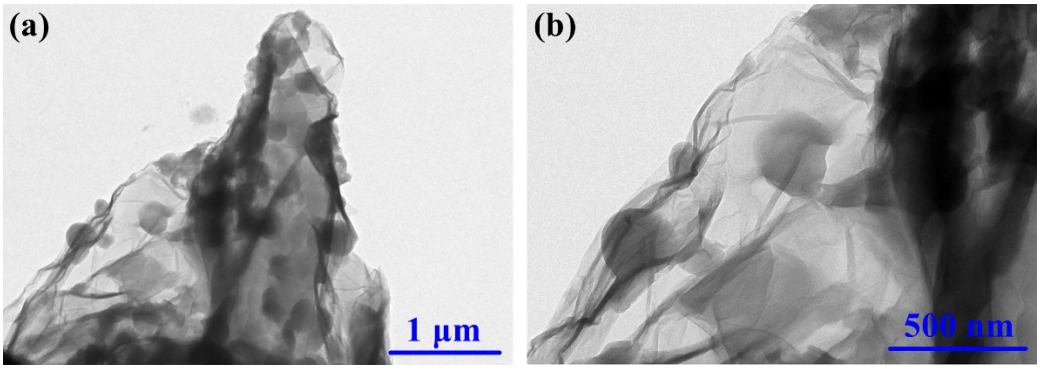

Fig. S2. (a,b) TEM images of the ZIF-67/GO.

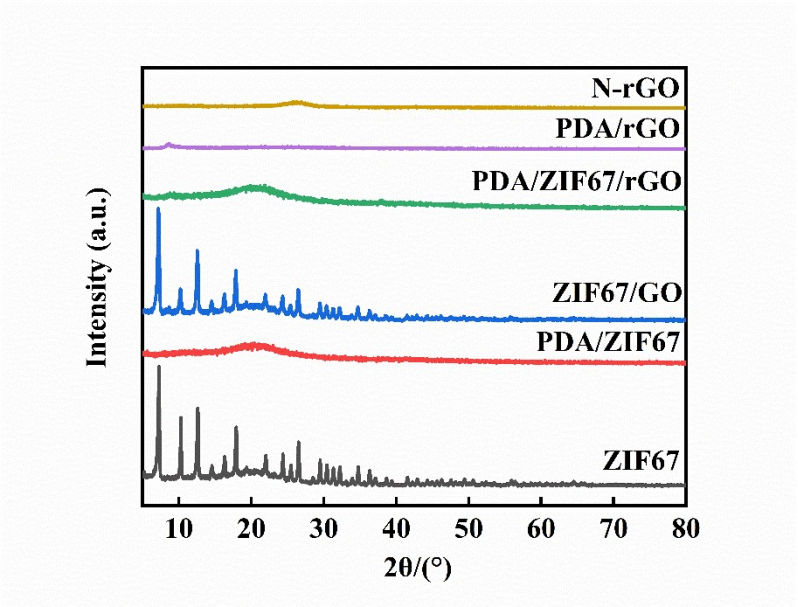

Fig. S3. XRD pattern of the samples.

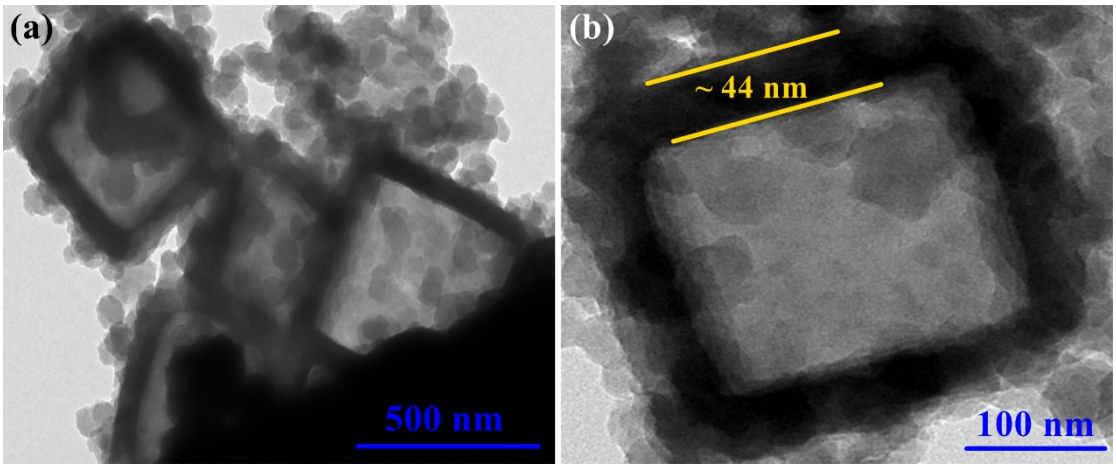

Fig. S4. (a,b) TEM images of the PDA/ZIF-67.

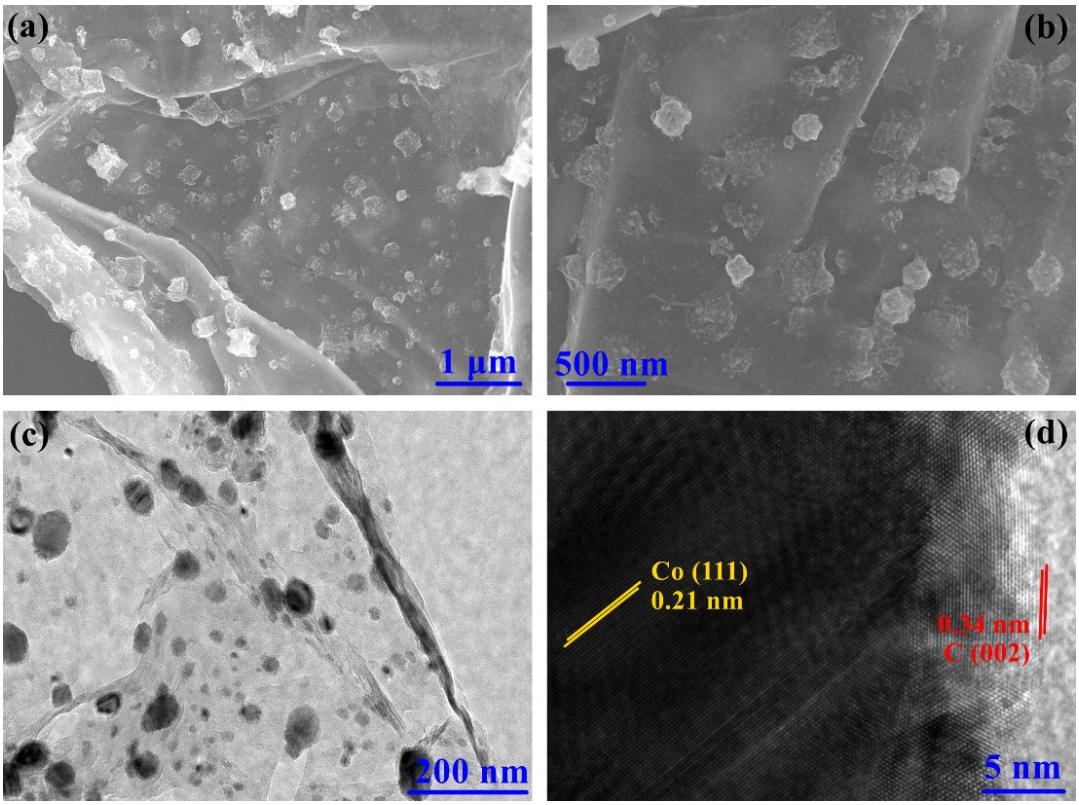

Fig. S5. (a,b) SEM, (c) TEM and (d)HRTEM images of the ZIF-67/GO.

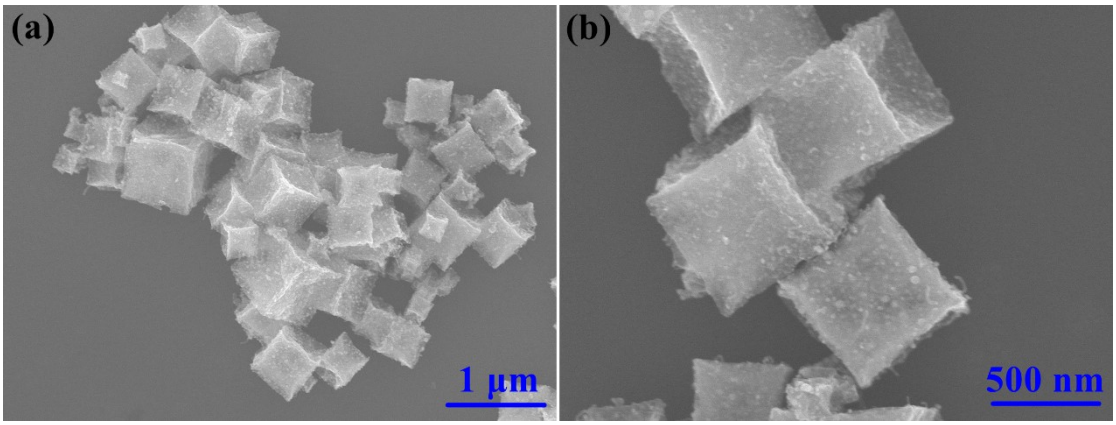

Fig. S6. (a,b) SEM images of the N-IC/Co.

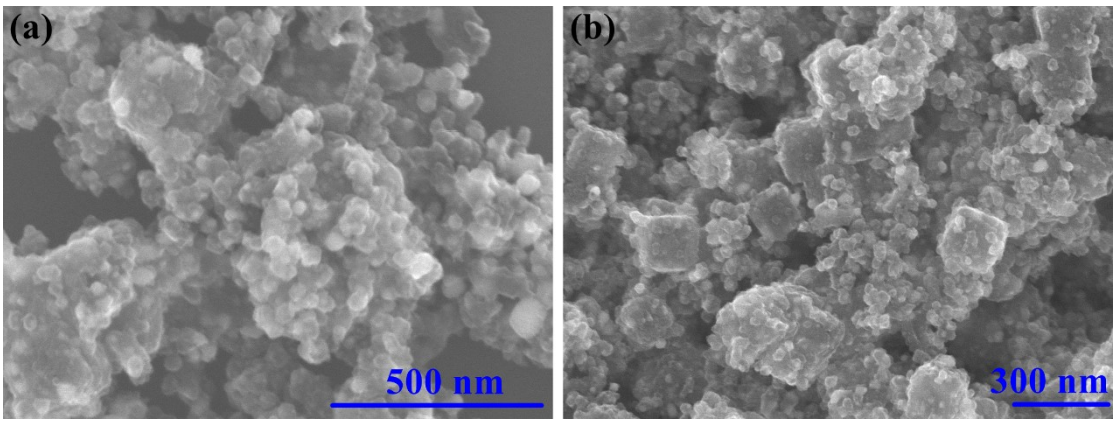

Fig. S7. (a,b) SEM images of the N-PC@IC/Co.

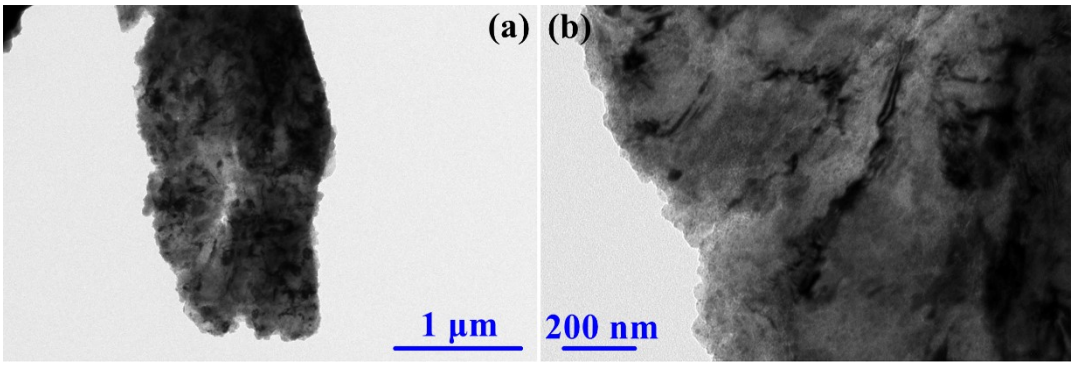

Fig. S8. (a,b) TEM images of the PDA/rGO.

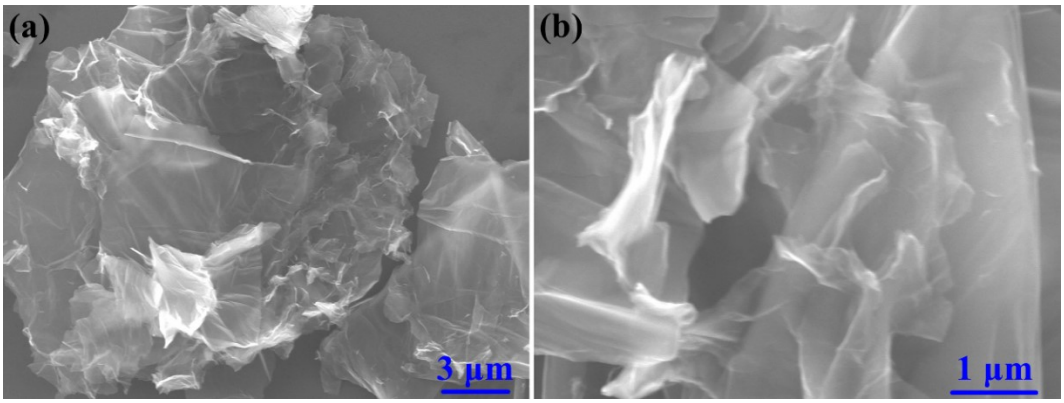

Fig. S9. (a,b) SEM images of the N-rGO.

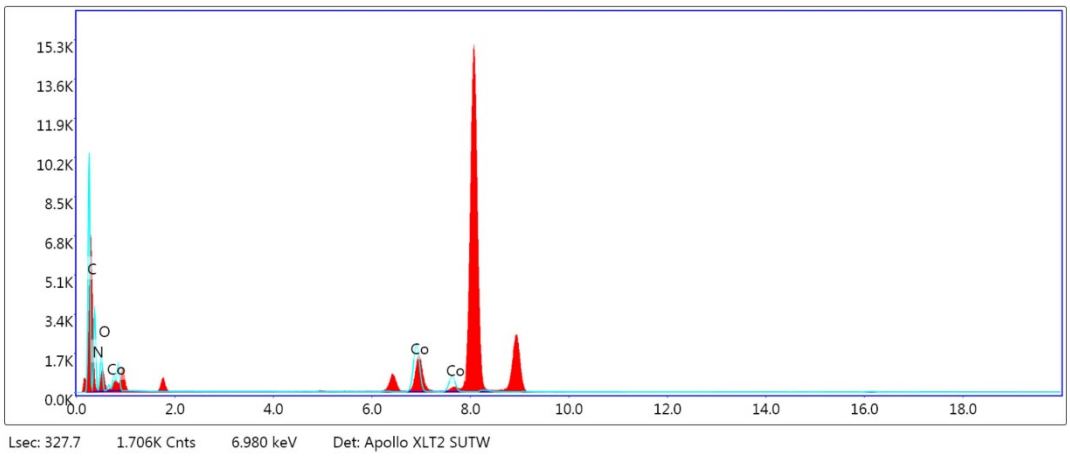

Fig. S10. TEM-EDS results of the N-PC@IC/Co/rGO.

Table S1 Detailed data of TEM-EDS for the N-PC@IC/Co/rGO

Element	Weight (%)	Atomic (%)	Net Error (%)
C K	39.36	55.21	0.48
N K	23.11	27.80	0.97
O K	8.16	8.59	1.62
Co K	29.37	8.40	0.74

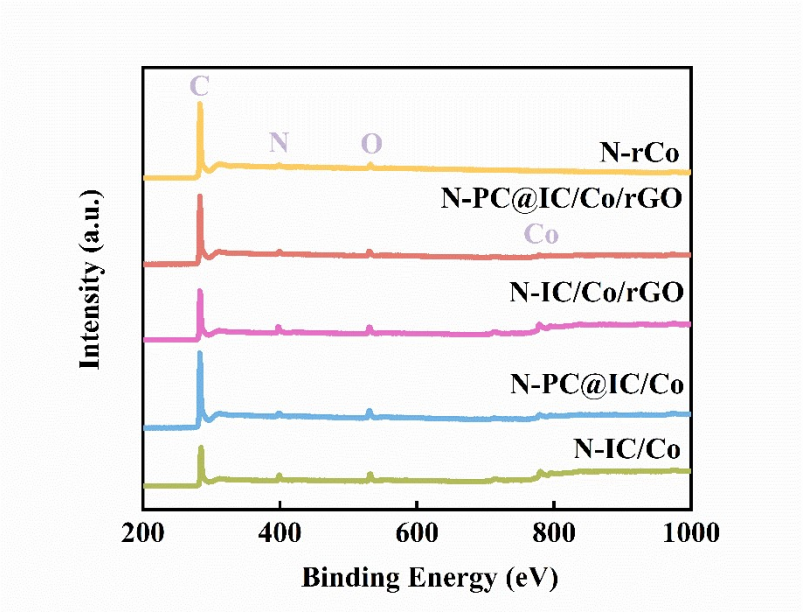

Fig. S11. The wide scan XPS spectra for samples.

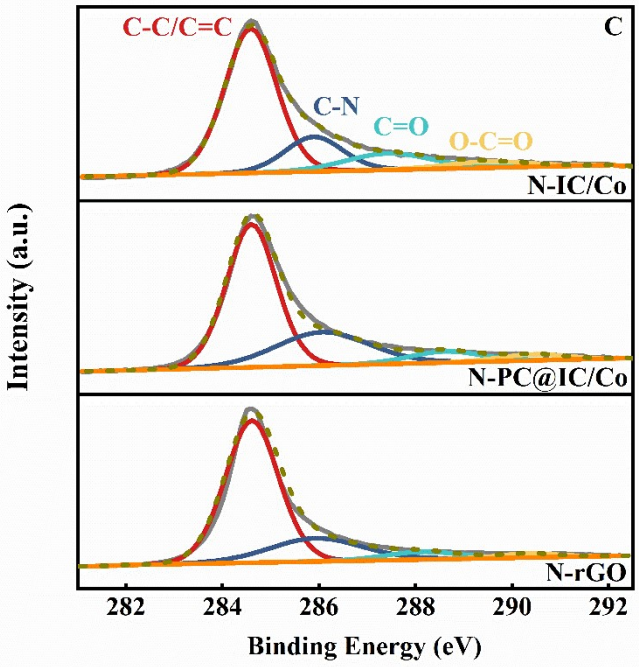

Fig. S12. The C 1s XPS spectra for samples.

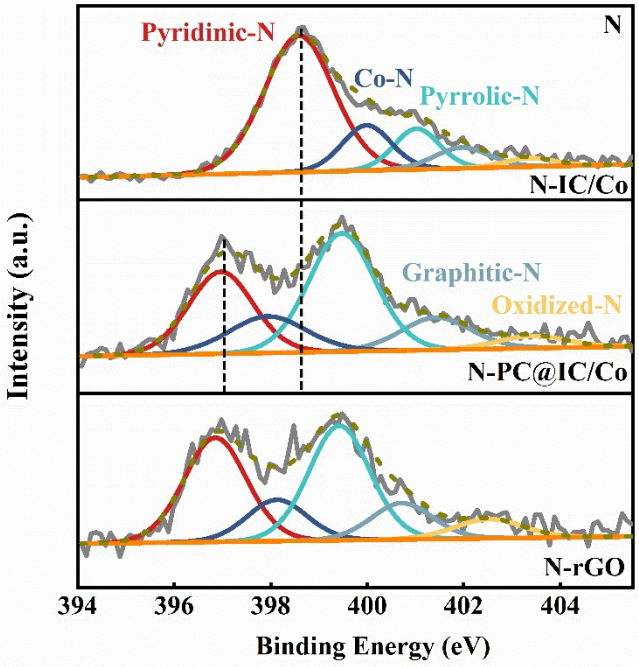

Fig. S13. The N 1s XPS spectra for samples.

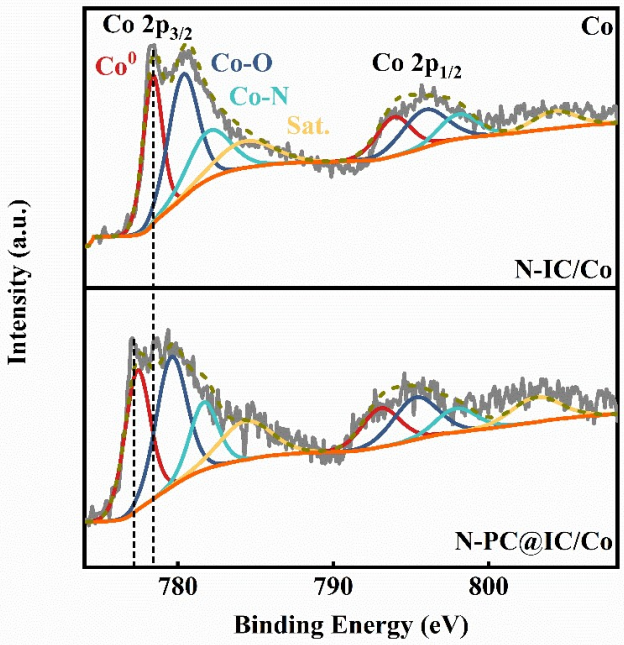

Fig. S14. The Co 2p XPS spectra for samples.

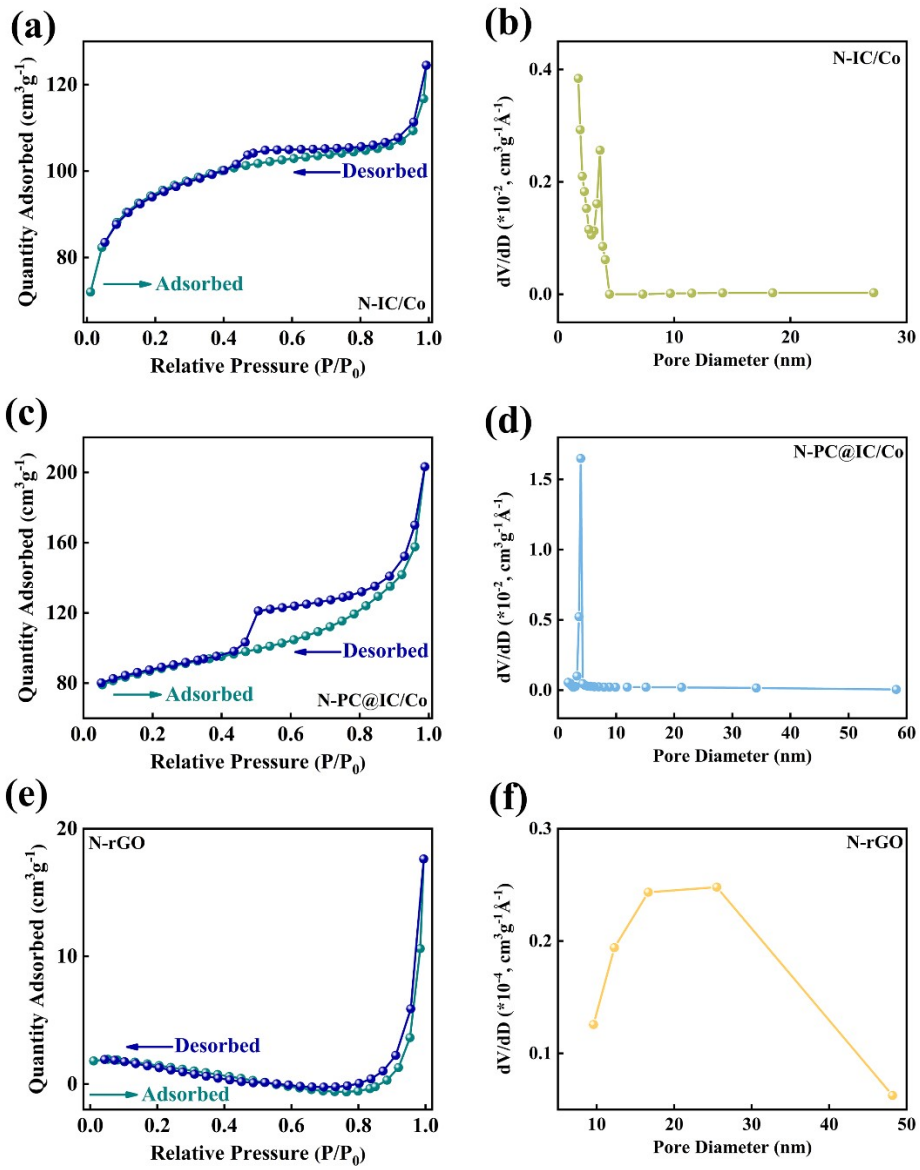

Fig. S15. N_2 adsorption-desorption isotherms and pore size distribution of the samples: (a,b) N-IC/Co, (c,d) N-PC@IC/Co and (e,f) N-rGO.

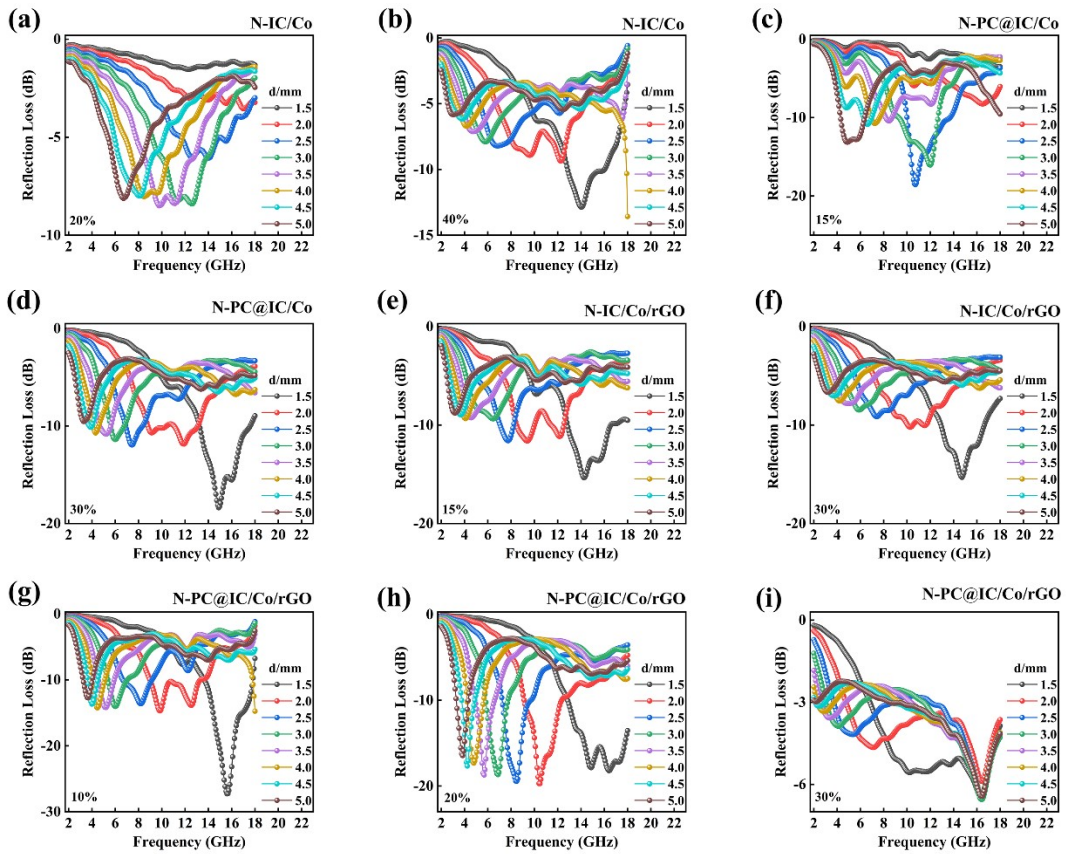

Fig. S16. Reflection loss curves of the samples with different thicknesses and filling ratio.

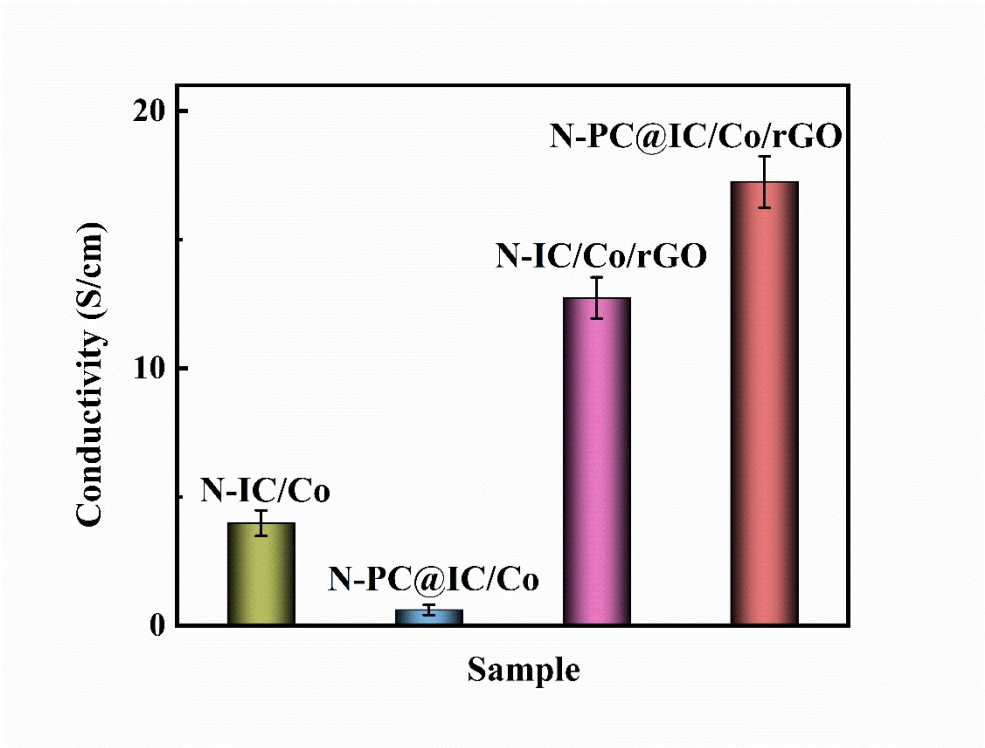

Fig. S17. Conductivity curves of the samples.

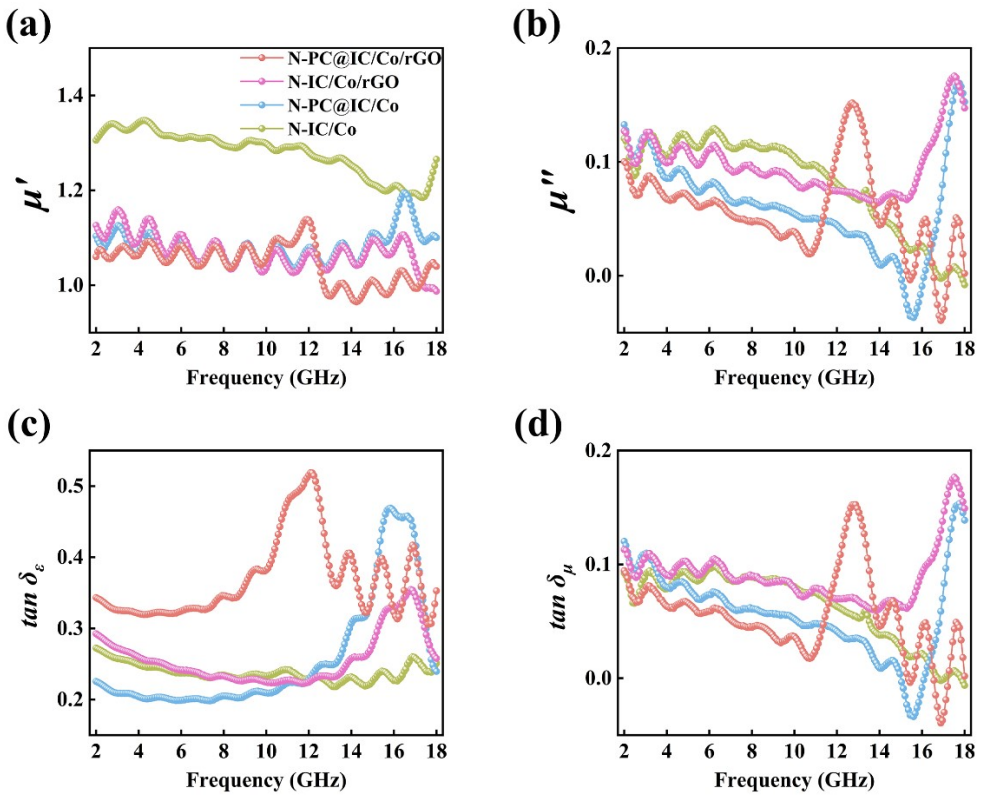

Fig. S18. (a) Real permeability, (b) imaginary permeability, (c) dielectric loss tangent and (d) magnetic loss tangent of the samples.

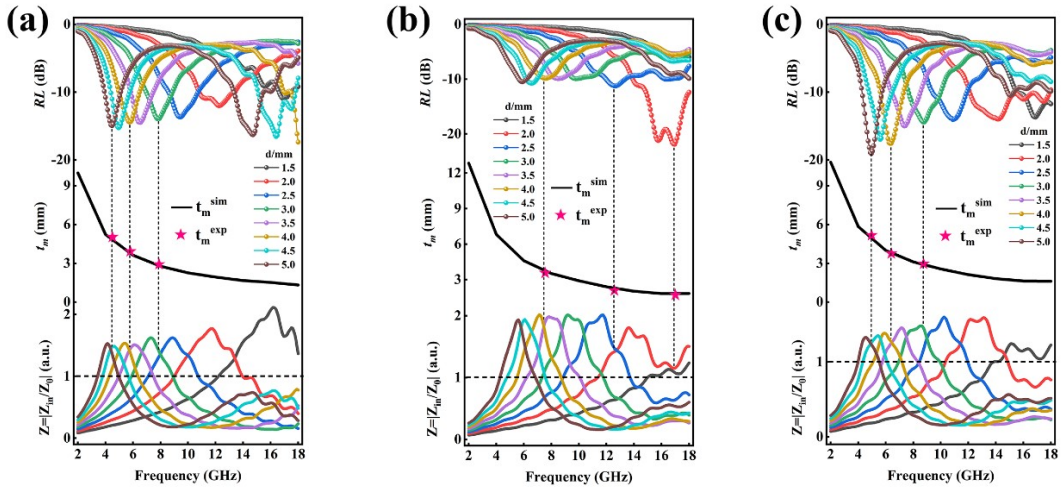

Fig. S19. Dependence of *RL* on frequency at 1/4λ thicknesses and the *Z* for the sample: (a) N-IC/Co, (b) N-PC@IC/Co and (c) N-IC/Co/rGO.

References

[1] H. Lv, Z. Yang, H. Pan, et al., *Prog. Mater. Sci.* **2022**, 127, 100946.

[2] X. Sun, J. He, G. Li, et al., *J. Mater. Chem. C* **2013**, 1, 765.

[3] T. Zhu, S. Chang, Y. Song, et al., *Chem. Eng. J.* **2019**, 373, 755.

[4] W. Liu, S. Tan, Z. Yang, et al., *Carbon* **2018**, 138, 143.

[5] J. Feng, Y. Zong, Y. Sun, et al., *Chem. Eng. J.* **2018**, 345, 441.

[6] Y. Zhou, S. Wang, D. Li, et al., *Composites, Part B* **2021**, 213, 108701.

[7] S. Lu, L. Xia, J. Xu, et al., *ACS Appl. Mater. Interfaces* **2019**, 11, 18626.

[8] X. Liang, B. Quan, J. Chen, et al., *ACS Appl. Nano Mater*. **2018**, 1, 5712.

[9] Y. Wang, X. Gao, X. Wu, et al., *Chem. Eng. J.* **2019**, 375, 121942.

[10] F. Wen, F. Zhang, Z. Liu, *J. Phys. Chem. C* **2011**, 115, 14025.

[11] J. Tang, N. Liang, L. Wang, et al., *Carbon* **2019**, 152, 575.

[12] L. Wang, X. Jia, Y. Li, et al., *J. Mater. Chem. A* **2014**, 2, 14940.

[13] G. Kresse, J. Furthmüller, *Comput. Mater. Sci.* **1996**, 6, 15.

[14] J. Perdew, K. Burke, M. Ernzerhof, *Phys. Rev. Lett.* **1996**, 77, 3865.

[15] P. Blöchl, *Phys. Rev. B* **1994**, 50, 17953.

[16] S. Grimme, J. Antony, S. Ehrlich, et al., *Chem. Phys*. **2010**, 132, 154104.

[17] K. Zhang, J. Chen, S. Yue, et al., *Composites, Part A* **2020**, 130, 105755.

[18] J. W. Crispin, A. L. Maffett, *Proceedings of the IEEE* **1965**, 53, 833.